University of Southampton
20/09/2010

FACULTY OF OCEAN AND
EARTH SCIENCES

HOW ARE MODE WATERS IN THE OCEAN FORMED ?

- Mathieu DEVER -

A dissertation submitted in partial fulfilment of the requirements for the degree of M.Sc. Physical Oceanography and Climate by instructional course.

Supervised by: Dr Alberto NAVEIRA-GARABATO,
and Dr Kevin OLIVER

National Oceanography Centre
NATURAL ENVIRONMENT RESEARCH COUNCIL

As the nominated University supervisor of this M.Sc. project by Mathieu DEVER, I confirm that I have had the opportunity to comment on earlier drafts of the report prior to submission of the dissertation for consideration of the award of M.Sc. Physical Oceanography and Climate.

Dr Alberto NAVEIRA-GARABATO Dr Kevin OLIVER

…….. …….

Acknowledgment

I would like to address special thanks to my supervisors, Alberto NAVEIRA-GARABATO and Kevin OLIVER, for their guidance and precious help during the project. I would also like to thanks all the people that made my work easier: David STEVENS and Mei LEE, who helped to get and understand HadGEM outputs, and Peggy COURTOIS for all the favours she kindly did.

Table of Content

Abstract

Mode Waters play a crucial role in the ventilation of the upper ocean. These water masses are characterized by a low Potential Vorticity (PV) signature. To understand the formation process of Mode Waters, the destruction of PV is studied using the flux form of the PV. Traditionally, this equation considered only an advective constituent, combined with a nonadvective constituent that arise from diabatic processes. The temperature difference between the ocean surface and the air just above increases or decreases the stratification, thus the PV. In recent studies, another nonadvective constituent, previously considered negligible, that arise from frictional forces has been emphasized. The Ekman drift coming from "downfront winds" puts light water on top of dense water in low latitudes, which creates an inward PV flux, and puts dense water on top of light water at mid-latitudes, which results in an outward PV flux. This study uses output from the low-resolution model HadGEM to investigate the contribution of each constituent and identify which process drives the formation of Mode Waters. A seasonal average study reveals that both constituents play a significant role in the destruction of PV. An hemispheric isopycnal analysis of these constituents during winter, the time of the year when Mode Waters form, show that the diabatic constituent tends to dominate in magnitude in the Northern hemisphere while the frictional constituent is principally responsible for the destruction of PV in the Southern hemisphere, especially in the vicinity of the ACC.

1. Introduction

Since the discovery of the Eighteen Degree Water by Worthington in 1959, Mode Waters have been identified in every ocean. They are classified in three different categories based on their location and potential density (Hanawa and Talley, 2001): While the Subtropical Mode Waters (STMWs) are associated with the western boundary current (Hanawa and Talley, 2001, Brambilla and Talley, 2008), the Eastern Subtropical Mode Waters (ESTMWs) are located equatorward of the subtropical front and to the west of the eastern boundary current (Wong and Johnson, 2003). The Subpolar Mode Waters (SPMWs) are associated with subpolar fronts on the poleward boundary of the subtropical gyres and are often the densest Mode Waters.

When Iselin (1939) published his model of water mass formation, Mode Waters have quickly been identified as a key component of the oceanic circulation in the upper kilometre of the ocean. Mode Waters, defined as "water of exceptionally uniform properties over an extensive depth range" (Glossary of Meteorology of the American Meteorological Society), are also spread over a very wide area over the upper ocean. The water masses are irreversibly subducted when the seasonal pycnocline becomes shallower in late winter (Stommel, 1979, Qiu and Huang, 1995). This subduction process and the advective spreading of these homogeneous waters in the upper ocean are relatively well understood and enhance the importance to improve our understanding of the mechanism of formation.

To be able to study the formation process of Mode Waters, it is crucial to use a viable tracer, or conserved property, that defined these waters. A lot of different parameters can be used such as the apparent oxygen utilization (Suga et al., 2008), the temperature or the density (Hanawa et al., 1988, Tsubouchi et al., 2009). But the potential vorticity (PV) is the most commonly used property. Often used either to trace water masses or to improve our understanding of ocean circulation (Talley and McCartney, 1982, Rhines and Young, 1982), PV is also very efficient to analyze the formation of Mode Waters. The low PV signature of these water masses suggests that the study of PV fluxes is crucial to

understand the destruction (construction), of PV, hence the creation (destruction) of Mode Waters. Traditionally, the sinks of PV are attributed to an anticyclonic wind stress curl, which is balanced by the friction at the western boundary current (Stommel, 1948), and a loss of buoyancy during wintertime (Worthington, 1977).

This loss of buoyancy during wintertime is the diabatic process often associated with Mode Waters formation. Indeed, cold-air outbreaks occurring at ocean surface during winter tend to cool the surface, which destroy the local stratification and lead to a PV loss. Conversely, if the ocean surface gets warmer, the local stratification increases, hence a gain in PV. This mechanism is the main reason why it is thought that Mode Waters are formed during winter, when the air above the ocean surface is the coldest and the seasonal pycnocline at its deepest. Then these particularly uniform waters subduct into the ocean interior when, during spring, the seasonal pycnocline becomes rapidly shallower.

But more recently, different studies have put forward another mechanism that could be responsible in the destruction of PV. While Chelton et al. (2001) detailed the close and complicated relationship between the ocean and the air just above, and how meso-scale oceanic phenomenon can have a significant impact on winds, Thomas (2005) discussed how “downfront” winds can play an important role in the destruction of PV. Winds blowing in the direction of a frontal jet (i.e. downfront winds) moves dense water on top of lighter water, which would decrease the stratification in this region and lead to a local PV loss. So besides the diabatic and advective components, the latest being responsible for the circulation and spreading of low-PV waters into the ocean interior and is not directly responsible for a global destruction or construction of PV, a frictional constituent can be added to the PV flux budget equation, that will be introduced later in the study.

The purpose of this study is to discuss the respective roles of the diabatic and frictional processes in the destruction of PV, or the creation of mode waters. The paper is structured as follows. In section 2, some background on the mathematics of PV flux is provided and the equations used to calculate the PV

budget and the contribution of each component of the PV flux are detailed. In this section, information about the type of data used for the study and the method chosen to proceed are also given. Section 3 explains the results obtained from the PV calculations as well as the frictional and diabatic calculations. Section 4 provides a discussion on the contribution of each constituent by comparing global seasonal maps of both components. Finally, section 5 gives a conclusion on the results obtained by this study and proposes openings for future work.

2. Data and method.

2.1 Data used

The data used for this study are outputs from the Hadley Centre Global Environmental Model (HadGEM). For the first phase of the study, a small sample of the data has been used to evaluate the code responsible of the calculation of the different components in the PV flux equation. This sample is composed of 5-days mean variables over two time step. The longitudinal component is a one-degree grid while the latitudinal component includes smooth transitions in the grid. It is a one-degree grid poleward of 30°N and 30°S, then decrease until it reaches a 0.9 degree grid at 20°N and 20°S and decrease again to a 0.6 degree grid at 10°N and 10°S to end up at a 1/3 degree grid at the equator (Figure 1). The grid along the z-axis is from the ocean surface to a depth of 148.5 m with a 10 m step.

For the second part of the study, once the code has been validated, more complete outputs from HadGEM are used. 5 days mean variables over 5 years are used, from the years 2064 to 2068. These years have been selected because of the fact that they are close to the end of the run, when the model is well spun-up. The National Oceanography Center of Southampton provided the data needed. The longitudinal and latitudinal grids are the same but the grid along the z-axis is from the ocean surface to 5000 m deep. The vertical grid is denser close to the surface (10 m steps) than at high depth (345 m steps)(Figure 2).

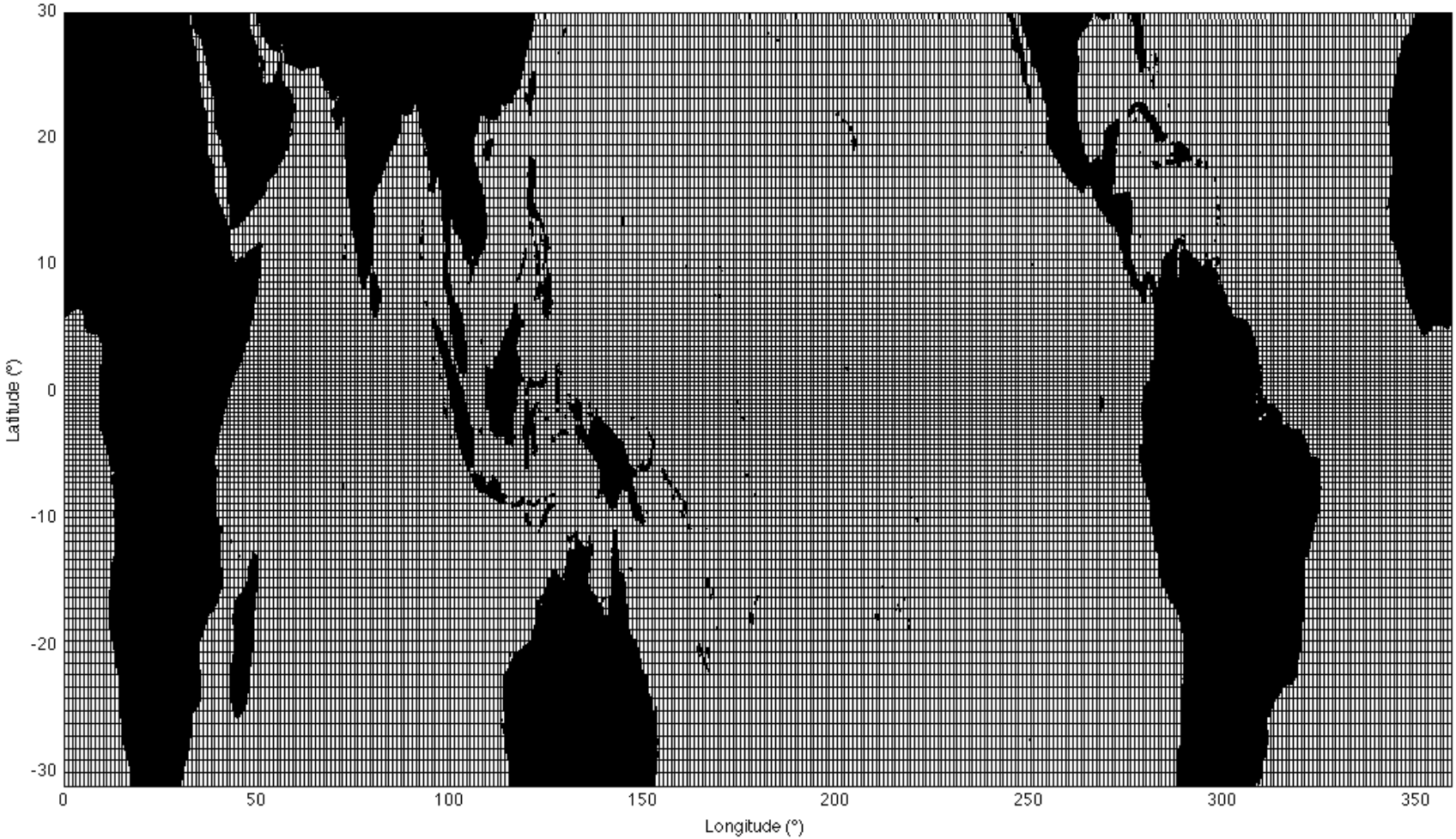

Figure 1: Longitudinal and latitudinal grids for HadGEM outputs. While the longitudinal grid is a 1-degree grid, the latitudinal grid becomes denser equatorward, starting from a one-degree grid at high latitudes to finish at a 1/3-degree grid at the equator.

2.2 Potential vorticity and its flux form

To understand and identify which atmospheric forcing conditions can reduce or increase the PV of the upper ocean, one must use the flux form of the PV equation. Through the literature, several equations of PV have been used, depending on the aims of the study. Here, the PV equation used comes from Marshall and Nurser (1992) and includes both the relative and planetary vorticity vectors. We will use the notation from Thomas (2005). Please note that in the following equations, vectors are designed with an arrow and denotes three-dimensional fields $\left(\vec{i},\vec{j},\vec{k}\right)$with $\left(\vec{i},\vec{j},\vec{k}\right)$ being the local zonal, meridional and vertical unit vectors. The PV equation becomes:

$$q = \vec{\omega}_a \cdot \nabla b \tag{1}$$

where $\vec{\omega}_a = f\vec{k} + \nabla \times \vec{u}$ is the absolute vorticity with f the coriolis parameter and $\vec{u}$ the velocity of the fluid; $b = -g\rho/\rho_0$ is the buoyancy with g the gravitational acceleration, ρ the density and ρ_0 the reference density. With this definition of the PV, we obtain a positive PV in the Northern Hemisphere and a negative PV in the Southern Hemisphere. As stated before, the flux form of the PV equation must be derived in order to identify the mechanisms responsible for the destruction of PV. Inspired from Thomas (2005), the PV flux can be defined as:

$$\vec{J} = q\vec{u} + \nabla b \times \vec{F} - D\vec{\omega}_a \tag{2}$$

As explained previously, the flux equation includes three components:

* An advective constituent $q\vec{u}$ which corresponds to the lateral advection of waters in the ocean interior at the surface and is not directly responsible for the destruction or creation of PV.

* A non-advective constituent $\nabla b \times \vec{F}$ that arise from frictional forces $\vec{F}$, defined as:

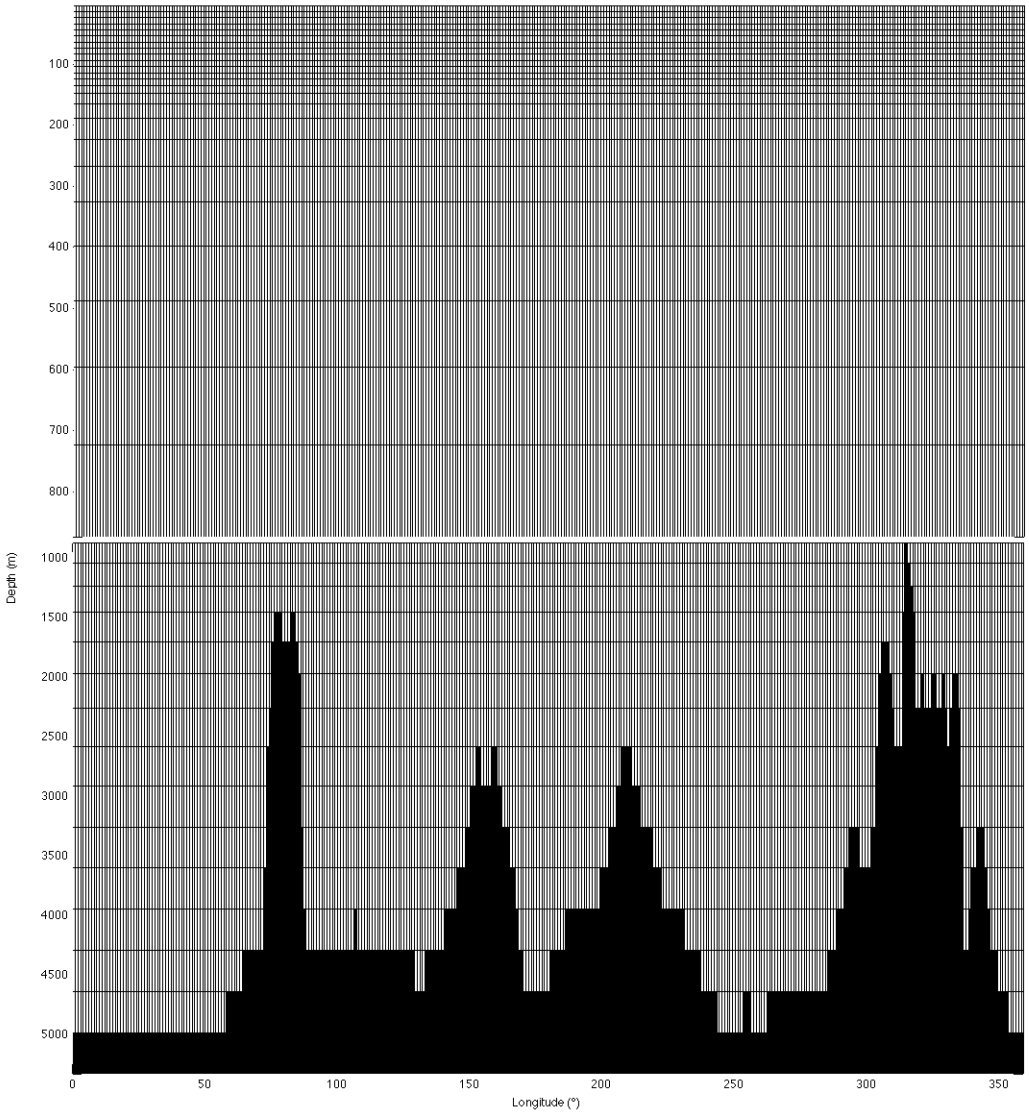

Figure 2: Vertical grids for the HadGEM outputs used. The grid along the z-axis is denser at the surface (10 m steps) than at high depth (up to 345 m steps).

$$\vec{F} \equiv \frac{D\vec{u}}{Dt} + f\vec{k} \times \vec{u} + \frac{1}{\rho_0}\nabla p + g\vec{k} \tag{3}$$

where $\frac{D\vec{u}}{Dt}$ denotes the Lagragian derivative of $\vec{u}$ and p is the dynamical pressure, determined via the hydrostatic equation (equation (12)). This non-advective constituent $\nabla b \times \vec{F}$ will be referred to in the following as the frictional component (Czaja and Hausmann, 2009).

* And a non-advective constituent $D\vec{\omega}_a$ that arise from diabatic processes D, defined as:

$$D \equiv \frac{Db}{Dt} \tag{4}$$

This constituent $D\vec{\omega}_a$ will be referred to as the diabatic component. It involves the exchange of heat and freshwater at the air-sea interface, so $\frac{Db}{Dt} \neq 0$.

Finally, any changes in PV is a result of a change in the convergence, or divergence, of the PV flux; that is,

$$\frac{\partial q}{\partial t} = -\nabla \cdot \vec{J} \tag{5}$$

The result of Haynes and McIntyre (1987) helps to simplify the calculation. Their "impermeability theorem" states that "isopycnal surfaces are impermeable to potential vorticity even in the presence of buoyancy forcing and frictional forces". This means that the PV content of an isopycnal layer can only vary when it intersects a boundary, such as the surface, the bottom or lateral boundaries of the ocean (Czaja and Hausmann, 2009). As Mode Waters are only present in the upper kilometre in the open ocean, this study focuses on the PV flux at the surface only. Thus, the net PV flux calculated does not need to be zero, as a positive (negative) PV flux can be balanced by a loss (gain) at an other type of boundary. Furthermore, the fact that this study considers PV flux across the ocean surface only means that only the vertical component of the PV flux equation is relevant (that is, if the reasonable approximation that the local ocean

surface normal is the same as $\vec{k}$ is made). Another approximation is that the vertical velocity, w, is zero at the ocean surface. Thus, equation (2) becomes:

$$\vec{J}_z = \left(-D\vec{\omega}_a\right)_{z=0} + \left(\nabla b \times \vec{F}\right)_{z=0} \cdot \vec{k} \tag{6}$$

which can be decomposed in the diabatic and frictional component, giving:

$$\vec{J}_z^{diab} = -\left(\frac{\partial v}{\partial x} - \frac{\partial u}{\partial y} + f\right)\left(\frac{Db}{Dt}\right)_{z=0} \tag{7}$$

and

$$\vec{J}_z^{fricst} = \left(\frac{\partial b}{\partial x}\vec{F}_{\vec{j}} - \frac{\partial b}{\partial y}\vec{F}_{\vec{i}}\right) \tag{8}$$

One must be aware that, as developed in Rhines (1993), the diabatic and frictional component cannot be directly quantitatively related to buoyancy flux and wind stress, respectively. From these definitions, one can expect an outward PV flux when there is a surface buoyancy loss $\left(\frac{Db}{Dt} < 0\right)$ or when there is a loss of stratification with a dense to light Ekman drift (Czaja and Hausmann, 2009).

2.3 Method

The method chosen for this study can be divided in two phases. The first phase was to use a small sample of data from HadGEM to evaluate the code in charge of the calculation of the diabatic and frictional components. Using only a small sample of data, over time and depth, makes the calculations faster and hence saves time in the evaluation phase of the study. The second one was the actual study, using the validated code to complete calculations in order to produce results that can be used to draw conclusions. Readers should note that relevant results of these evaluation tests will be included in section 3.

The first phase was made of series of tests to see if any mistakes were included in the code. The first one of these tests was to verify the integrity of the sample of the data used by calculating the cell budget for a conservative property directly output by the model such as the Salinity. Once this has been verified and

validated, the calculation of PV has been made and, as PV is a conservative property, the PV cell budget has been checked. Cell budgets calculation used the simple equation of conservation:

$$\mathcal{V}\frac{\partial C}{\partial t} = \sum_{n=1}^{n=6} \mathcal{A}_n \vec{u}_n C_n \tag{9}$$

where $\mathcal{V}$ is the volume of a cell, C is the conservative property, n is the number of faces of the cell, $\mathcal{A}_n$ is the area of the face, $\vec{u}_n$ is the velocity through the center of the face, and C_n is the conservative property at the center of the face considered. Care must be taken for the area of a face, as explained in section 2.a., the grids are not linear which makes some cells not cubic.

Some other minor tests have been run to check if the method used to calculate the spatial and time derivatives is right. The horizontal spatial derivatives have been validated using the geostrophic balance in the model. The equations of geostrophic balance are:

$$fv = \frac{1}{\rho_0}\frac{\partial p}{\partial x} \tag{10}$$

and

$$-fu = \frac{1}{\rho_0}\frac{\partial p}{\partial y} \tag{11}$$

where f is the Coriolis parameter, u and v are the zonal and meridional velocities, ρ_0 is the reference density, and p is the dynamic pressure.

The time derivatives have been validated through the use of the hydrostatic equation:

$$p = \rho g H + p_0 \tag{12}$$

where ρ is the density, H is the depth, and p_0 is the surface pressure. The time derivative of (12) becomes:

$$\frac{\partial p}{\partial t} = \rho g w \tag{13}$$

where w is the vertical velocity.

Once the calculation of PV has been validated via the cell budget and derivatives have been checked, the last step in the validation process was to verify equation (5). The purpose of this test was to evaluate the calculations of the different PV flux components.

The second phase was to use complete outputs from HadGEM to obtain seasonal maps of each non-advective component of the PV flux equation. The frictional and diabatic component have been calculated over 5 years, from 5-days mean variables, and then averaged by month then season. Winter designates the months of December, January and February; Spring includes the months of March, April and May; Summer is composed by the months of June, July and August and, finally, Autumn includes September, October and November. The years selected are from 2064 to 2068, intentionally chosen at the end of the run, to make sure that the model is well spun up.

3. Results

3.1 PV budget test

Equation (2) has been verified on both the data sample and the outputs used for the actual study. Both the left-hand-side and right-hand-side of this equation have been independently calculated and plotted. The results obtained from the data sample show some undeniable similarities, proving that there is no major mistakes in the calculations of PV and advective and non-advective components of the PV flux equation. Although, because of the fact that the data sample only includes one time-step, the results do not perfectly match. The same process has been applied to the month of August of the first year (2064), where several time-steps were available. Anticipating on the results, the two sides of the equation should be perfectly identical, as the 6 time steps of the month of April allow a more precise calculation. Figure 3 and Figure 4 shows the results from the calculations of both sides of equation (2) at the ocean surface. One can easily notice that both maps are almost identical; they show the same features and have the same order of magnitude of 1.10^{-10} s^{-4}. White cells have no value

attached and black ones represent land. A red color means an entry of PV into the evaluated cell while a blue color is synonym of an extraction of PV from the cell. Care must be taken, a blue color for example does not necessary mean that there is an upward PV flux and that PV is being destructed by either diabatic or frictional processes. This map includes the advective constituent of the PV flux equation. The blue can be explained by a local destruction of PV via an upward flux through the ocean surface as well as by a simple re-distribution of PV via local advection.

That being said, two minor differences can be noticed. The first one is the width of the white stripes along land. Indeed, close to the land, there is more cell with no value attached in the map of the divergence of the PV flux than in the map of the time-derivative of PV. That is due to the boundary conditions used in the calculation. The calculation of PV only involves one level of derivation: velocities and density are only spatially derived once to obtain the PV. If the PV flux and PV budget equations (equation (2) and equation (5)) are closely examined, equation (2) involves one level of derivation, as well as equation (5). This double level of derivation when calculating the divergence of $\vec{J}$ has the effect of extending the width of the white stripes running along land cells.

The other minor variation is a difference of the patterns observed within 10° of the equator, both North and South. To be more precise, the features observed in this region are nearly the same on both maps but the extent and magnitude are a bit different. The fact that none of the maps present a systematic difference compared to the other shows that these variations does not come from coding problems. The causes of these differences has not been investigated, as the equator is not a region of interest. Indeed, no mode waters is created in the vicinity of the equator.

3.2 Potential vorticity maps

The results of the PV calculations are presented in Figure 5(5.a is winter, 5.b spring, 5.c summer and 5.d autumn). As explained in section 2, the PV has the sign of f, that is positive in the Northern Hemisphere and negative in the

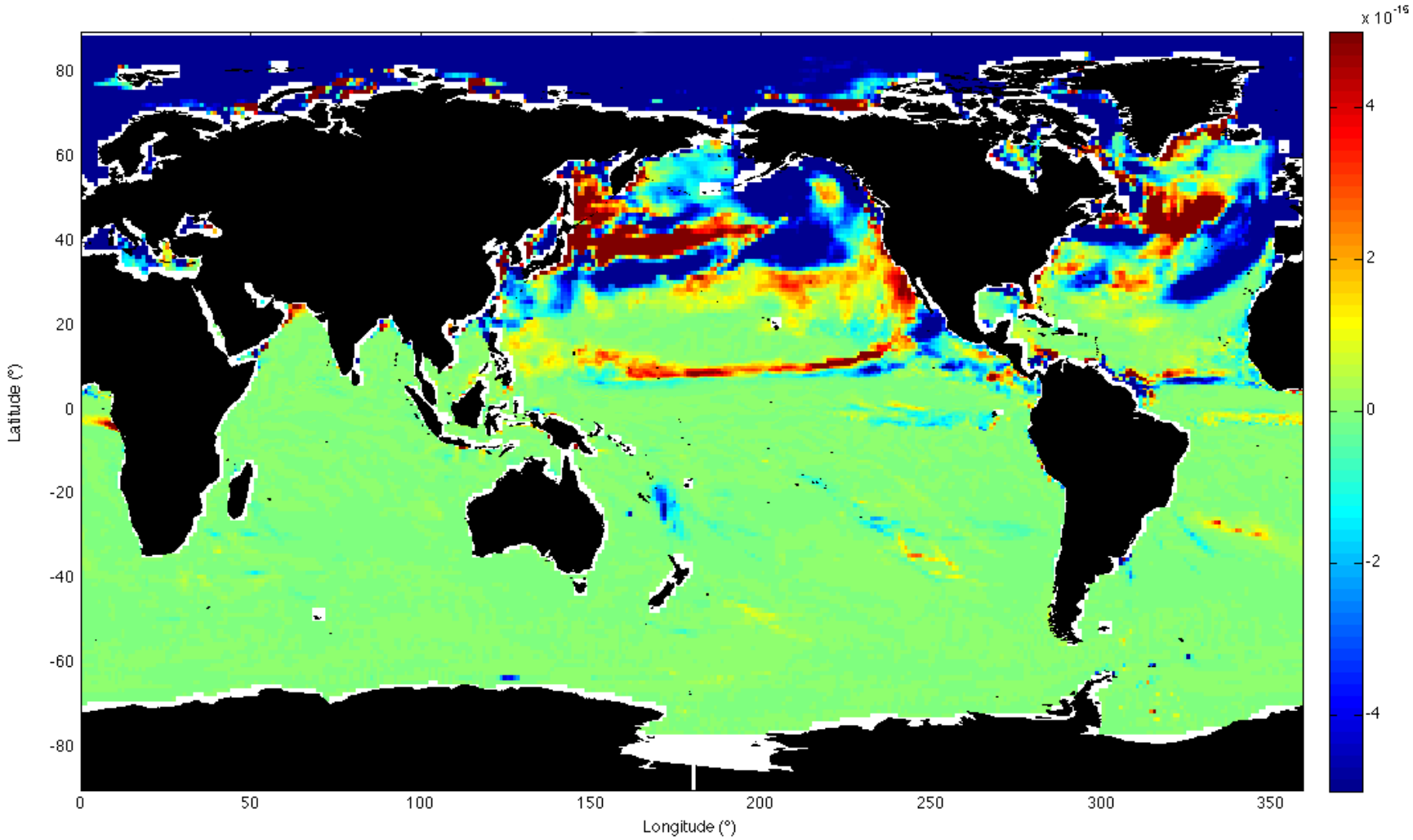

Figure 3: Left-Hand-Side of equation (5), that is the temporal derivative of the PV during the month of August 2064; in units of s^{-4}.

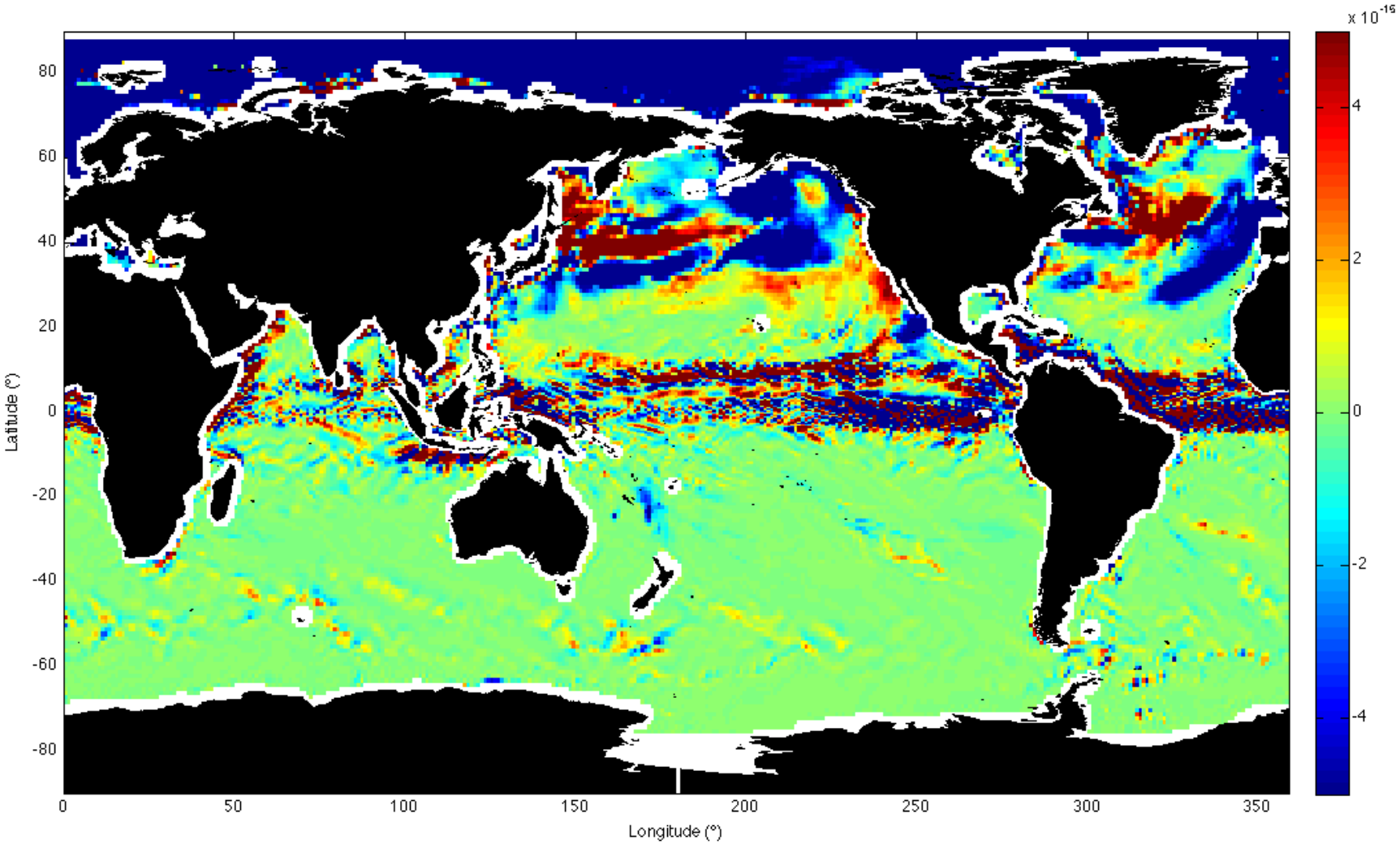

Figure 4: Right-Hand-Side of equation (5), that is minus the divergence of the total PV flux at the surface during the month of August 2064; in units of s^{-4}.

Southern Hemisphere. To make the results clearer, the seasonal maps of PV show the absolute value of PV, to avoid confusion with a meaningless sign difference. Indeed, negative PV does not make sense on the physic point of view and what is important for the study is to identify the regions of low PV compared to regions with a higher PV. While observing Figure 5, it can be noticed that a specific time and spatial variability occurs. Figure 5.a and 5.c show that during local winter, the PV tends to be a lot smaller than during the local summer. Indeed, Figure 5.a shows that during winter in the Northern hemisphere and summer in the Southern hemisphere, PV tends to be a lot higher in the Southern regions, regions where it is summer, than in the Northern regions, where it is winter. Figure 5.c confirms this observation: when seasons are reversed, the high PV regions are now located in the Northern Hemisphere and low PV regions in the Southern.

If one focuses on the Northern Hemisphere first, it can be noticed that an annual variation occurs. PV starts low in winter, increases slightly during spring to be really high during summer and then decreases again during autumn, to be low during the next winter. On a spatial point of view, the Northern hemisphere does not present any specific spatial variation during winter. On the other hand, there are some regions where PV increases first during spring. The Sea of Okhotsk (North of Japan) where it shifts from 5.10^{-9} s^{-3} to 12.10^{-9} s^{-3} is one of them. Another one is located south of the Kuroshio current where a tongue a high PV (8 to 10.10^{-9} s^{-3}) appears from about 125°E to 160°W (200°E) and between 30°N and 40°N. A last patch of high PV is located in the center of the North-Atlantic subtropical gyre. These patches are then included in the high PV regions that appears during summer, which include the entire Northern Hemisphere located North of 20°N. That being said, three places keep a low-PV even during Summer. The PV close to the South West coast of United States increases only slightly (about 1.10^{-9} s^{-3}) while the surrounding region double to triple its magnitude. The same phenomenon happens around the South-East of Greenland. The PV then decreases during autumn and, once again, PV in some regions does not decrease as fast as most of the Northern Hemisphere. These regions are not the same as the ones where PV increased first during spring. They are located in the middle of the subtropical gyre in the Pacific ocean and off the coast of Labrador.

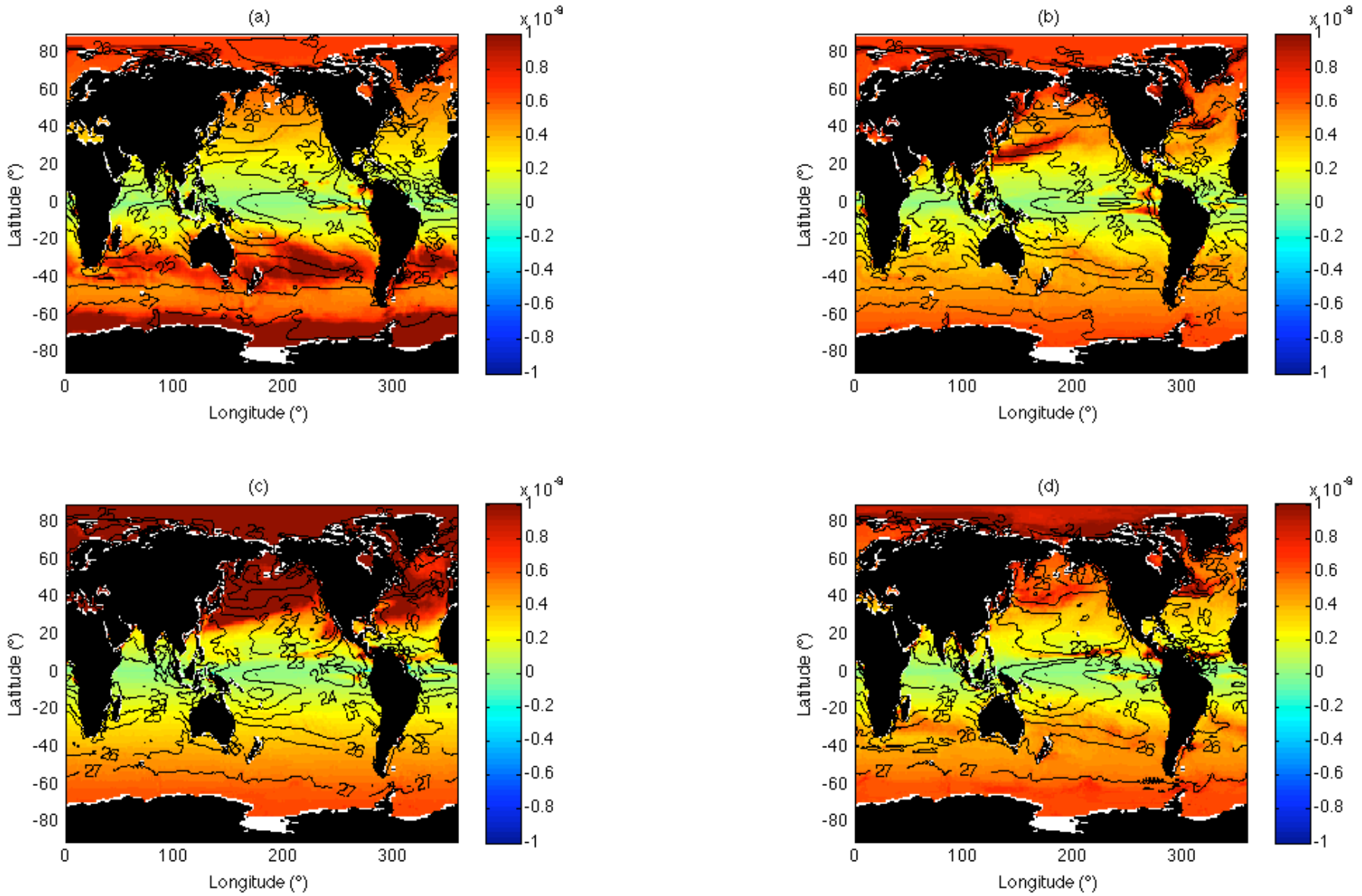

Figure 5: Seasonal mean of the modulus of the Potential Vorticity (PV) at the sea surface in the Northern hemisphere (a) winter, (b) spring, (c) summer and (d) autumn; in units of s^{-3}; superimposed on the seasonal mean density minus 1000 $kg.m^{-3}$ (contoured every 1 $kg.m^{-3}$).

The same annual variability can be observed in the Southern hemisphere. During the austral winter, no special pattern of high, or low, PV can be observed. During the austral spring, regions of high PV start to appear in the vicinity of 30°S and 60°S. Still, some regions located in these latitude do not experience the same increase in PV: The water located at the cape of Good Hope still has a low-PV signature, so has the water off the coast of Brazil. During the austral summer, high-PV regions appear at the same latitude as during the austral spring. Around 30°S, the same regions keep their low-PV signature. The Cape of Good Hope still has a low-PV signature, as well as waters off the North West coast of Australia and Chile and off the North East coast of Australia. A stripe of high-PV is located all along the south pole, from 60°S to 70°S. During the austral autumn, the PV of these high-PV regions diminishes. Some very light features are still present around 30°S. These features will disappear with the austral winter.

Two precise patterns need to be stressed: the low-PV signature of the major currents (Agulhas, gulf stream, Kuroshio and Brazil currents) all year around, and the stripe of low-PV between 40°S and 60°S in the Southern Hemisphere.

3.3 Frictional contribution to surface PV flux

a. Seasonal maps

The seasonal mean value of the frictional contribution to the surface PV flux (J_s^{frict}) is plotted in Figure 6. The most obvious spatial pattern that can be observed in figure 6 is the change of sign with latitude. Indeed PV exits (red part of the color spectrum) around mid-latitudes, that is from 30° to 60° in both hemispheres and enters the ocean at low latitudes, that is between 10° and 30° from the equator in both hemispheres. This spatial pattern is not affected by seasonal variation, only the extent of these positive or negative regions change a bit with the seasons. For example, the upward PV flux that exists around the Antarctic Circumpolar Current (ACC) begins around 40°S and ends at 60°S during the local summer and begins at lower latitudes (around 30°S) during the local winter. This region also tends to be a bit bigger in magnitude that the other regions over the year. While this southern region has a magnitude mostly contained between $0.5.10^{-13}$ m.s^{-4} and 2.10^{-13} m.s^{-4}, the other regions have generally a magnitude contained between $0.5.10^{-13}$ m.s^{-4} and 1.10^{-13} m.s^{-4}.

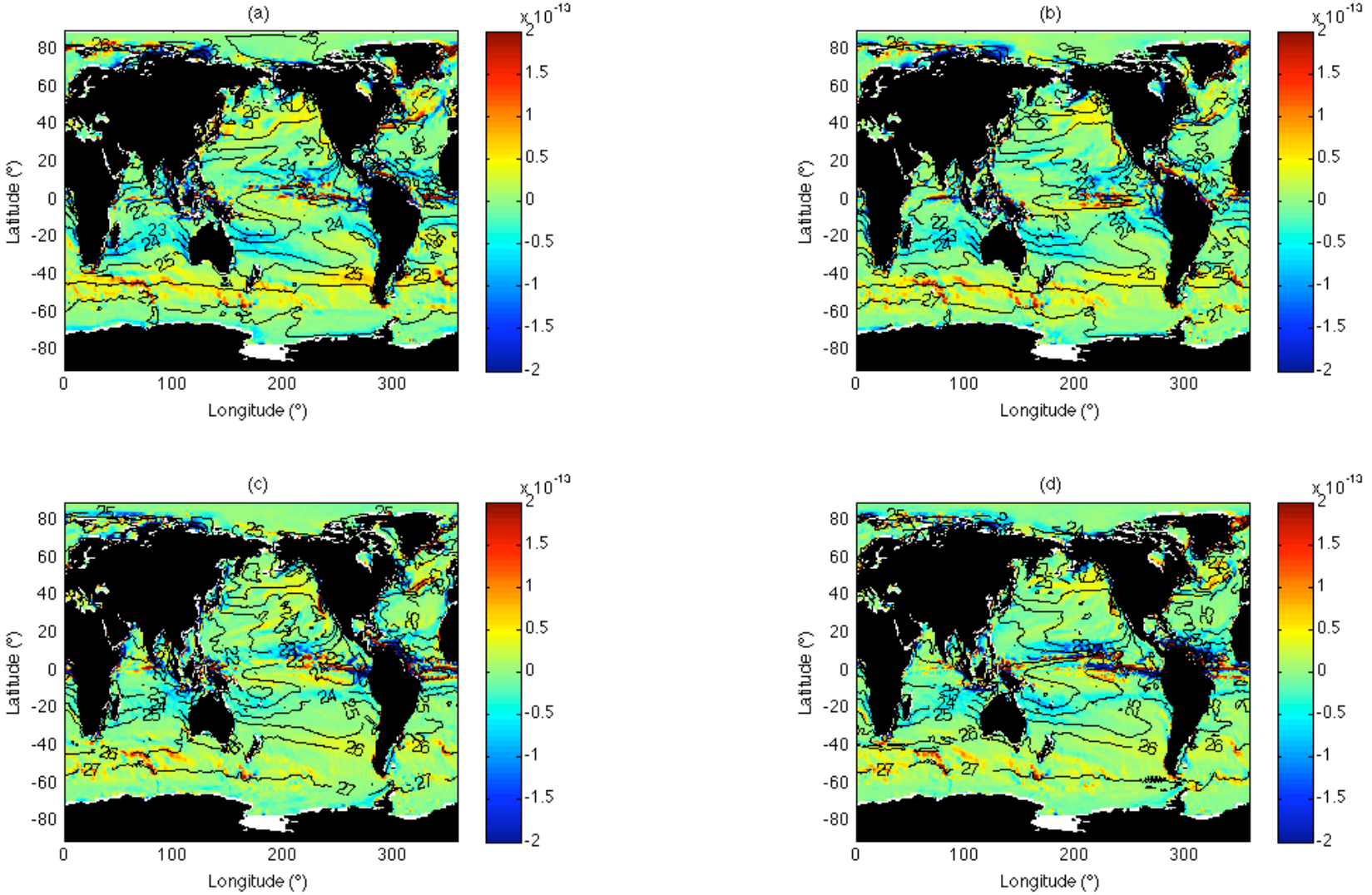

Figure 6: Seasonal mean frictional contribution (J_s^{frict}) to the sea surface PV flux in N.H. (a) winter, (b) spring, (c) summer and (d) autumn; in units of $m.s^{-4}$; superimposed on the seasonal mean density minus 1000 $kg.m^{-3}$ (contoured every 1 $kg.m^{-3}$). A positive value indicates PV destruction.

There are two main temporal variations in J_s^{frict} . The first one is, as explained before, the change in latitude of the boundary between regions with a positive and a negative PV flux. The second one is the seasonal change in magnitude of the PV flux. Indeed, the PV flux due to friction tends to increase during local autumn and winter. For example, the region with a positive PV flux in the northern hemisphere is mainly contained between 0 $m.s^{-4}$ and $0.5.10^{-13}$ $m.s^{-4}$ during summer (figure 6.c) and is equal or superior to $0.5.10^{-13}$ $m.s^{-4}$ during winter (figure 6.a). This phenomenon also occurs in the Southern hemisphere, even though it is less obvious.

b. Isopycnal analysis

An isopycnal analysis is also an interesting way to look at the results due to the "impermeability theorem" (cf section 2.2). Seasonal isopycnals positions are indicated in figure 6. It is important to track the outcropping isopycnals as they experienced a wide meridional and zonal variation depending on the season.

Figure 7 and figure 8 show the isopycnal analysis in the Northern and Southern Hemispheres for the frictional contribution to the PV flux across the sea surface. Figure 7 has interesting features: First of all, the sign of the frictional PV flux tends to change along the year for a given density. Second, the amplitude of J_s^{frict} does not vary a lot: it is roughly contained between 0 and $0.9.10^{-13}$ $m.s^{-4}$. The biggest change in magnitude is located between 1023 $kg.m^{-3}$ and 1024 $kg.m^{-3}$. Finally, one must realise that the strong patterns close to 1021 $kg.m^{-3}$ must not be taken into consideration as they come from cells located in semi-closed seas and not from the open ocean.

The isopycnal analysis for the Southern Hemisphere (figure 8) has differences and similarities. The main difference is that it shows a PV entry (negative values) for isopycnals smaller than 1024 $kg.m^{-3}$, and a PV exit (positive values) for water denser than 1024 $kg.m^{-3}$. That means that, unlike the isopycnal analysis for the Northern Hemisphere, the PV flux keeps the same sign all year around for a given isopycnal. On the other hand, the amplitude of J_s^{frict} in the Southern Hemisphere is similar. At low densities (i.e. ≈1022 $kg.m^{-3}$), the PV entry can reach a magnitude of about 2.10^{-13} $m.s^{-4}$ while, at high densities (i.e. ≈1025-1026 $kg.m^{-3}$), PV exit is about 0.7 $m.s^{-4}$. Once again the strong features around 1021 $kg.m^{-3}$ are due to data from semi-closed regions,

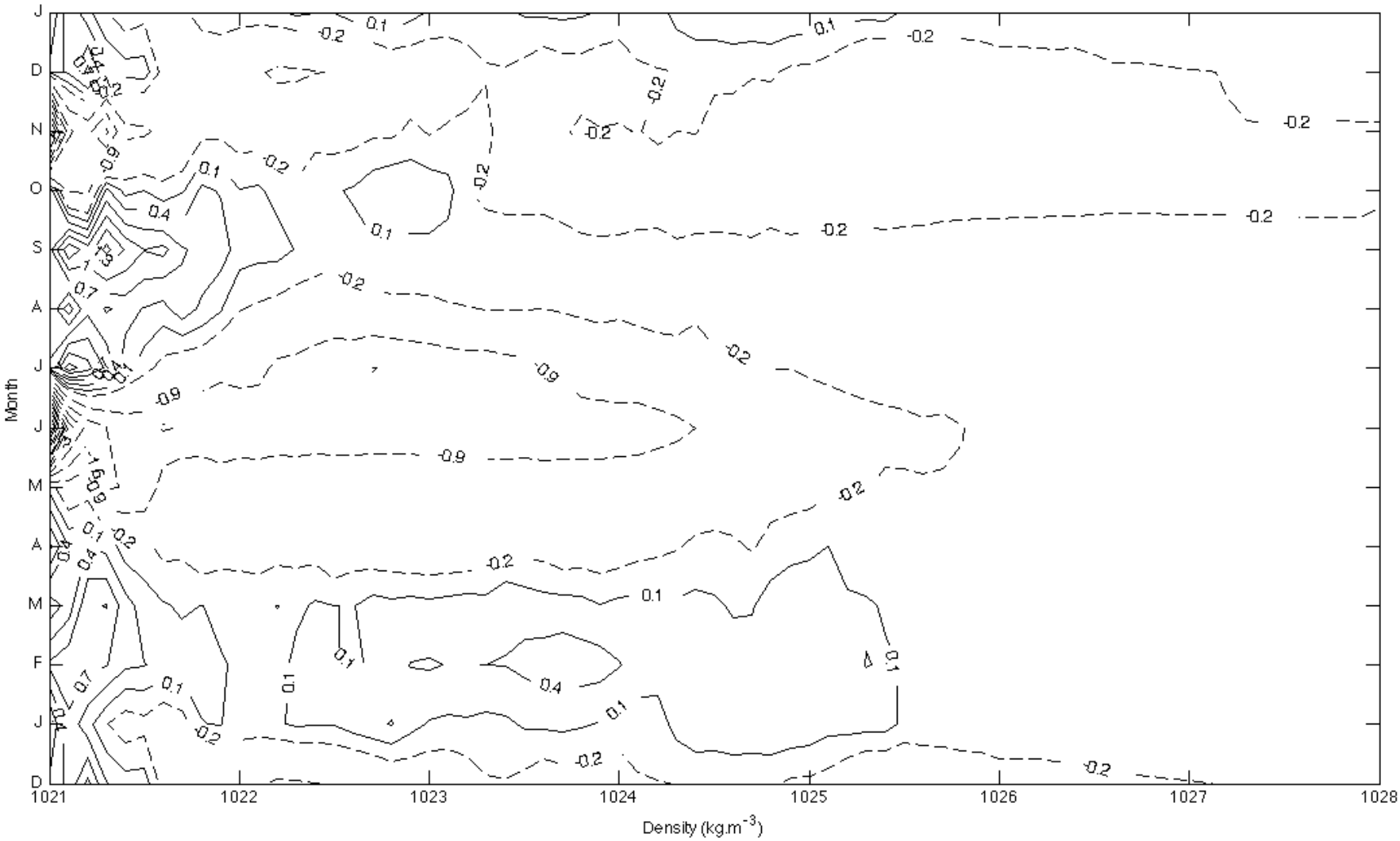

Figure 7: Isopycnal analysis for the monthly mean J_s^{frict} in the Northern Hemisphere, in units of 10^{-13} m.s^{-4}. A positive value (solid line) indicates PV destruction and a negative value (dashed line) represents a PV entry.

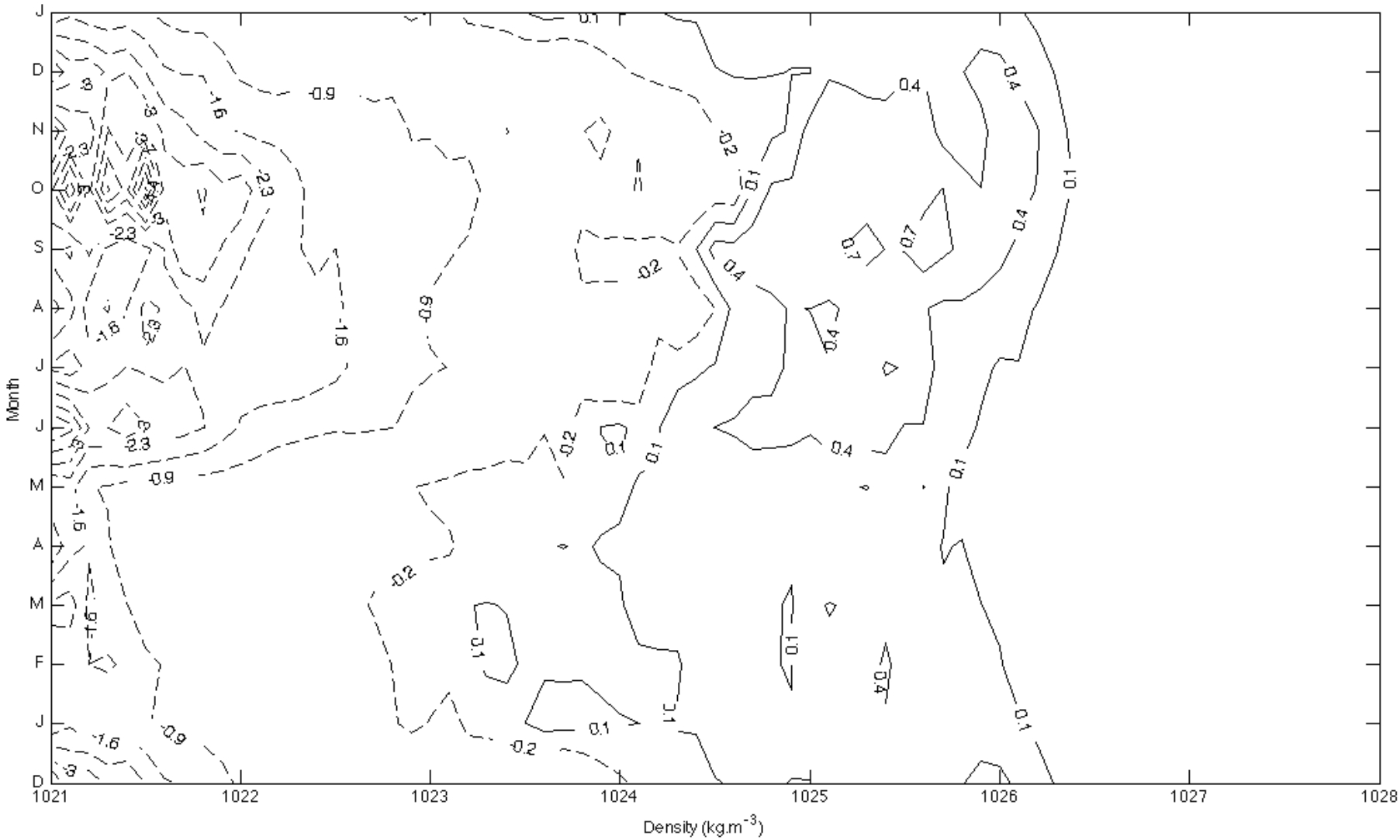

Figure 8: Isopycnal analysis for the monthly mean J_s^{frict} in the Southern Hemisphere, in units of 10^{-13} m.s^{-4}. A positive value (solid line) indicates PV destruction and a negative value (dashed line) represents a PV entry.

included in the model output, not from the open ocean.

The last part of the isopycnal analysis is displayed in figure 9. The winter mean PV flux due to friction was computed for both hemispheres (January to April for the Northern Hemisphere and from July to October for the Southern Hemisphere). The behaviour of the two hemispheres is very different. The Northern Hemisphere shows an almost flat line, very close to zero. As it can be seen in figure 6, some outcropping isopycnals experience both positive and negative PV flux depending on the time of the season. These two fluxes can cancel each others out and have a result of a relatively flat line when averaged over a couple of month. The wintertime mean in the Southern Hemisphere presents a lot more variations. Isopycnal corresponding to a lower density than 1024.5 $kg.m^{-3}$ experience a negative PV flux (PV entry) that increases as the density decreases. It reaches -2.10^{-13} $m.s^{-4}$ around 1021.5 $kg.m^{-3}$. Waters with a density between 1024 $kg.m^{-3}$ and 1026.5 $kg.m^{-3}$ are subject to a positive annual mean PV flux that can reach $0.5.10^{-13}$ $m.s^{-4}$. For even higher densities, the annual mean PV flux is close to zero, slightly negative, for both hemispheres.

3.4 Diabatic contribution to surface PV flux

a. Seasonal maps

Figure 10 represents the seasonal mean of the diabatic contribution to the PV flux across the ocean surface. Immediately, spatial patterns can be noticed. First of all, it has to be noticed that the two hemispheres have generally opposite sign all year long, which is consistent with what we would expect, as the two hemispheres experience opposite seasons. Second of all, one can see that the diabatic PV flux (J_s^{diab}), whatever its sign, decreases equatorward. Indeed, during every seasons, J_s^{diab} is very small close to the equator and in both hemispheres. Third of all, for each season, a "stripe" of low J_s^{diab} appears in the Southern Hemisphere from 40°S to 60°S. The diabatic PV flux along this "stripe" is always smaller than $0.5.10^{-13}$ $m.s^{-4}$ in magnitude, while water surrounding it always experience a flux with a magnitude bigger than $0.5.10^{-13}$ $m.s^{-4}$, positive or negative depending on the season. Finally, it can be noticed that the major currents over the globe all experience an important diabatic PV flux, once again, with the sign changing with seasons.

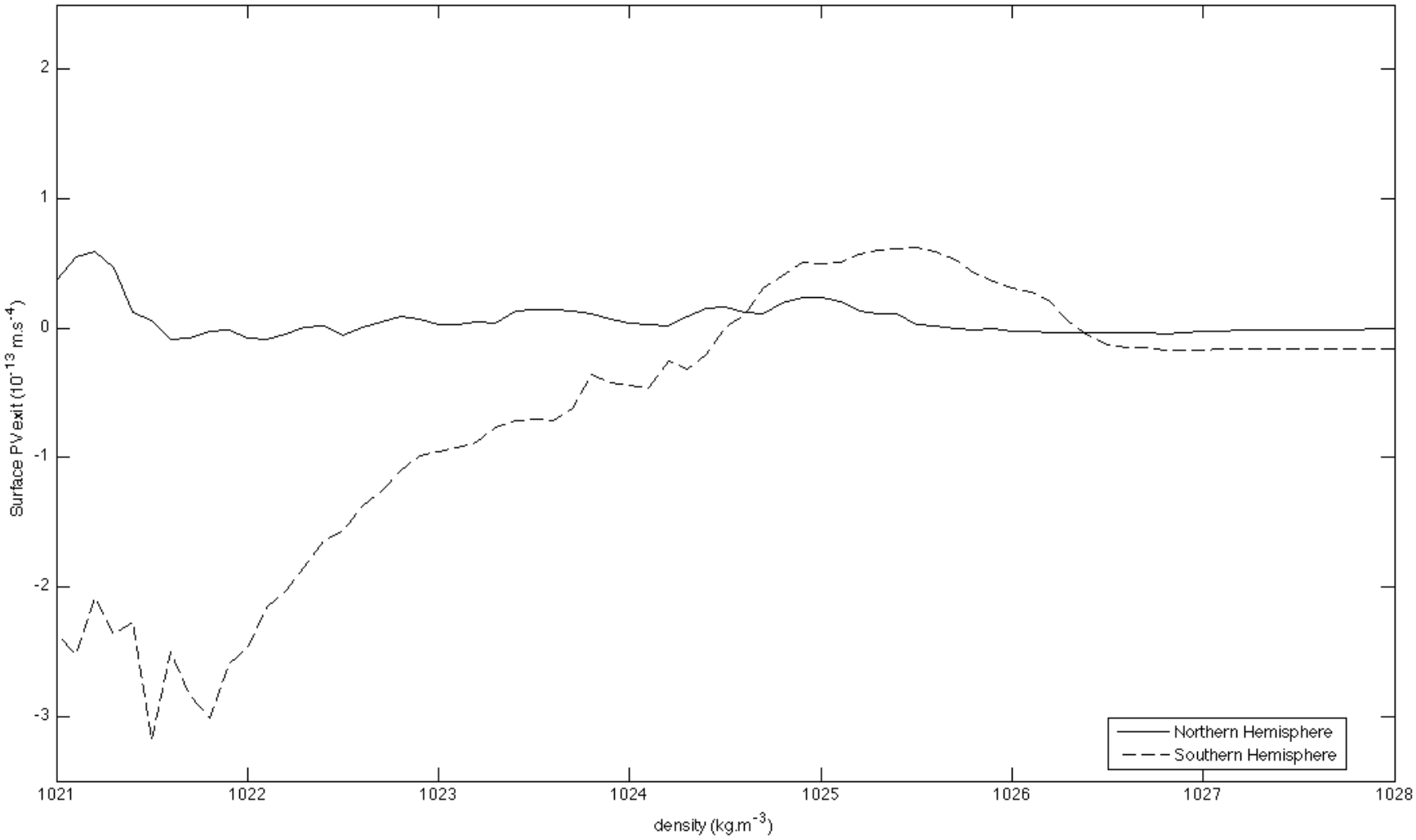

Figure 9: Surface PV exit due to friction (J_s^{frict}) averaged for the month of January to April for the Northern Hemisphere and from July to October for the Southern Hemisphere; in units of 10^{-13} m.s^{-4}. Solid line is the Northern Hemisphere, dashed line is the Southern Hemisphere. A positive value indicates PV exit.

Some seasonal variability obviously occurs. The main one is the change in the direction of the PV flux. J_s^{diab} tends to be positive during a local autumn and winter and then positive during the local spring and summer, observation valid for both hemispheres. If one focuses on the winter season (figure 10.a for Northern Hemisphere and figure 10.c for Southern Hemisphere), it can be noticed that a strong flux is present in the vicinity of major currents. The Kuroshio and Gulf Stream currents are highly visible in figure 10.a and the Agulhas current is also characterized by a high PV flux region in figure 10.c. It reflects the large wintertime buoyancy loss over these regions (Czaja and Hausmann, 2009). Another feature that is interesting on these maps is the fact that, for a given season, the diabatic PV flux has a bigger magnitude in the Northern Hemisphere than in the Southern Hemisphere. Indeed, if figure 10.b and figure 10.d are compared, we see that J_s^{diab} is a lot bigger in the Northern Hemisphere during local autumn (figure 10.d) than in the Southern Hemisphere during the local autumn (figure 10.b). Finally, if the maps are observed a bit further, a zone of bigger amplitude relative to its surrounding tends to appear on the East side of each oceanic basin. This pattern has also been observed in Czaja and Hausman (2009) and attributed to the "*slow descent of dry air over the ocean in the subsidence branch of the Hadley-Walker circulation".* These regions can be observed close to the Baja California, to the west coast of Northern Africa and along the western coastline of South America.

b. isopycnal analysis

The isopycnal analysis has been conducted the same way for the diabatic contribution to the surface PV flux. Figure 11 shows the PV flux associated for each outcrops through the year, averaged over the 5 years used for the study, for the Northern Hemisphere. This figure confirms the change of sign with the seasons noticed in figure 10. For almost every isopycnals, except for the very low densities (ρ< 1022 kg.m^{-3}), there is a PV entry from April to August, and a PV exit the rest of the year. For densities smaller than 1022 kg.m^{-3}, an upward diabatic PV flux occurs all year long, even though it is very small in magnitude from April to August. Diabatic PV exit peaks at a $1.6.10^{-13}$ m.s^{-4} in the vicinity of 1023 kg.m^{-3} in October and the diabatic PV entry can reach a magnitude of $1.5.10^{-13}$ m.s^{-4} in July for densities contained between 1024.5 kg.m^{-3} and 1027 kg.m^{-3}.

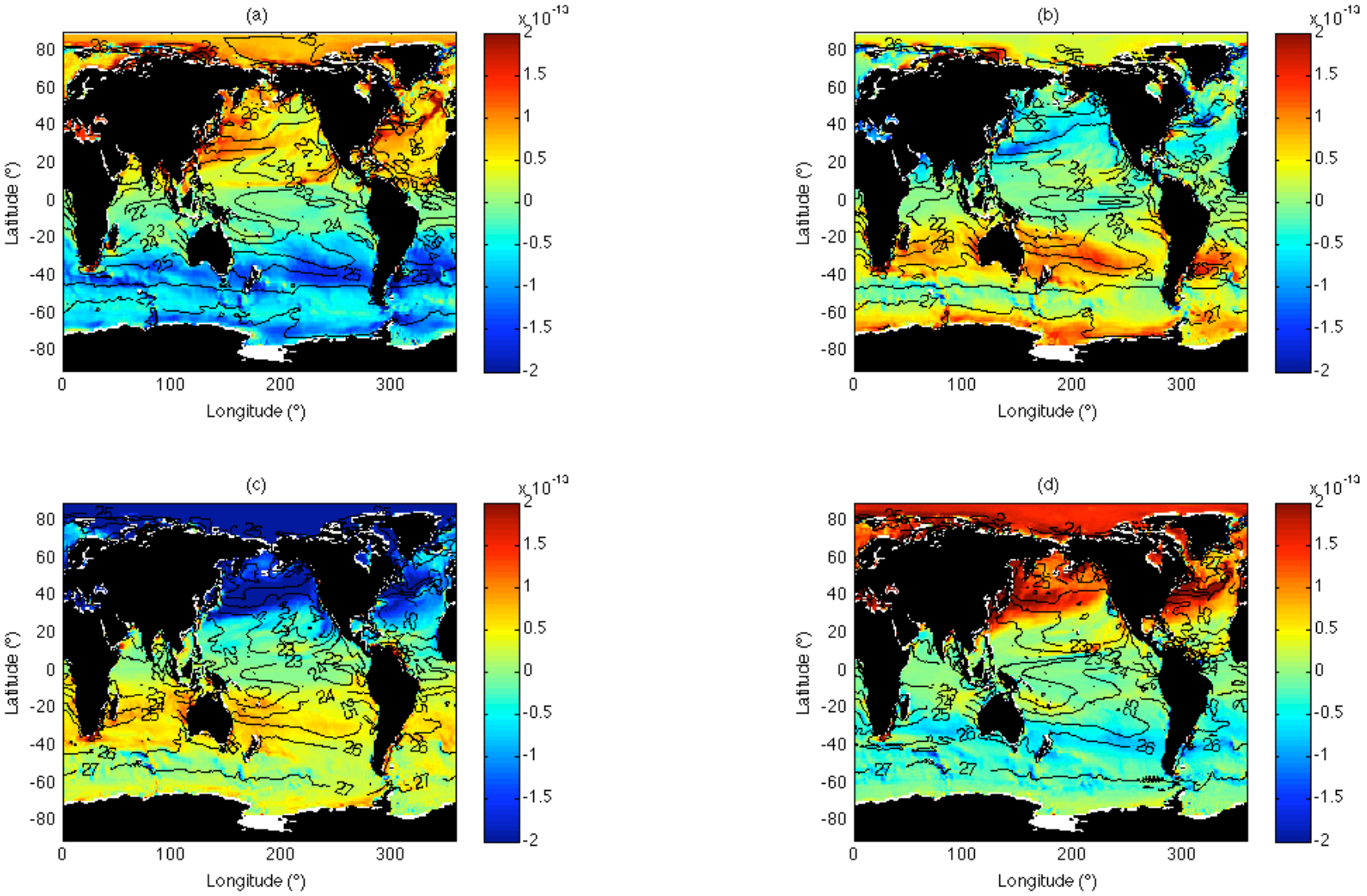

Figure 10: Same as in figure 6, but for the seasonal mean diabatic contribution J_s^{diab} across the sea surface for N.H. (a) winter, (b) spring, (c) summer and (d) autumn.

The isopycnal analysis of J_s^{diab} for the Southern Hemisphere (figure 12) is similar to the Northern Hemisphere (figure 11). Once again, the direction of the diabatic PV flux changes through the year. As detailed above, the two hemispheres have a flux in opposite directions for a given month. That is why outcrops denser than 1023 $kg.m^{-3}$ experienced a positive flux during the austral winter, that is from March to August and a negative flux (PV entry) through the rest of the year. Outcrops lighter than this threshold have a positive diabatic PV flux (PV exit) all year around, with, as seen in figure 11, a weakened magnitude, close to zero, during the austral summer, that is from September to February.

The magnitude of this diabatic contribution to the surface PV flux is smaller for the Southern than for the Northern Hemisphere. Indeed the upward J_s^{diab} (PV exit) peaks only at 1.10^{-13} $m.s^{-4}$ for a very narrow density range (1026 $kg.m^{-3}$ to 1026.2 $kg.m^{-3}$) in October when its maximum in the Northern Hemisphere is $1.5.10^{-13}$ $m.s^{-4}$ and is spread over a range of 2.5 $kg.m^{-3}$. The same phenomenon occurs for the downward component of J_s^{diab} (PV entry): It peaks in the same region of density (around 1023 $kg.m^{-3}$) but with a magnitude of only $0.6.10^{-13}$ $m.s^{-4}$, almost three times less than in the Northern Hemisphere.

Finally, figure 13 shows the diabatic PV flux (J_s^{diab}) averaged from the months of January to April for the Northern Hemisphere and from July to October for the Shouthern Hemisphere. The first thing that is important to notice in this result is that, as detailed in the analysis of figures 11 and 12, the Northern Hemisphere experienced a bigger upward PV flux than the southern Hemisphere for the whole density range. Another important detail is the fact that, as expected, the Northern Hemisphere is subject to an upward flux (PV exit) over wintertime for all outcrops, with a magnitude $0.8.10^{-13}$ $m.s^{-4}$ for low densities (1023$kg.m^{-3}$ to 1024 $kg.m^{-3}$) and around $0.25.10^{-13}$ $m.s^{-4}$ for higher densities.

The Southern Hemisphere is generally dominated by an upward diabatic PV flux (PV exit) over the winter, except for densities contained between 1024 $kg.m^{-3}$ and 1026.5 $kg.m^{-3}$. It reaches a maximum magnitude of $0.3.10^{-13}$ $m.s^{-4}$ around 1022 $kg.m^{-3}$ and a minimum of $-0.5.10^{-13}$ $m.s^{-4}$ around 1025.5 $kg.m^{-3}$. For densities denser than 1026.5 $kg.m^{-3}$, the diabatic contribution is very small.

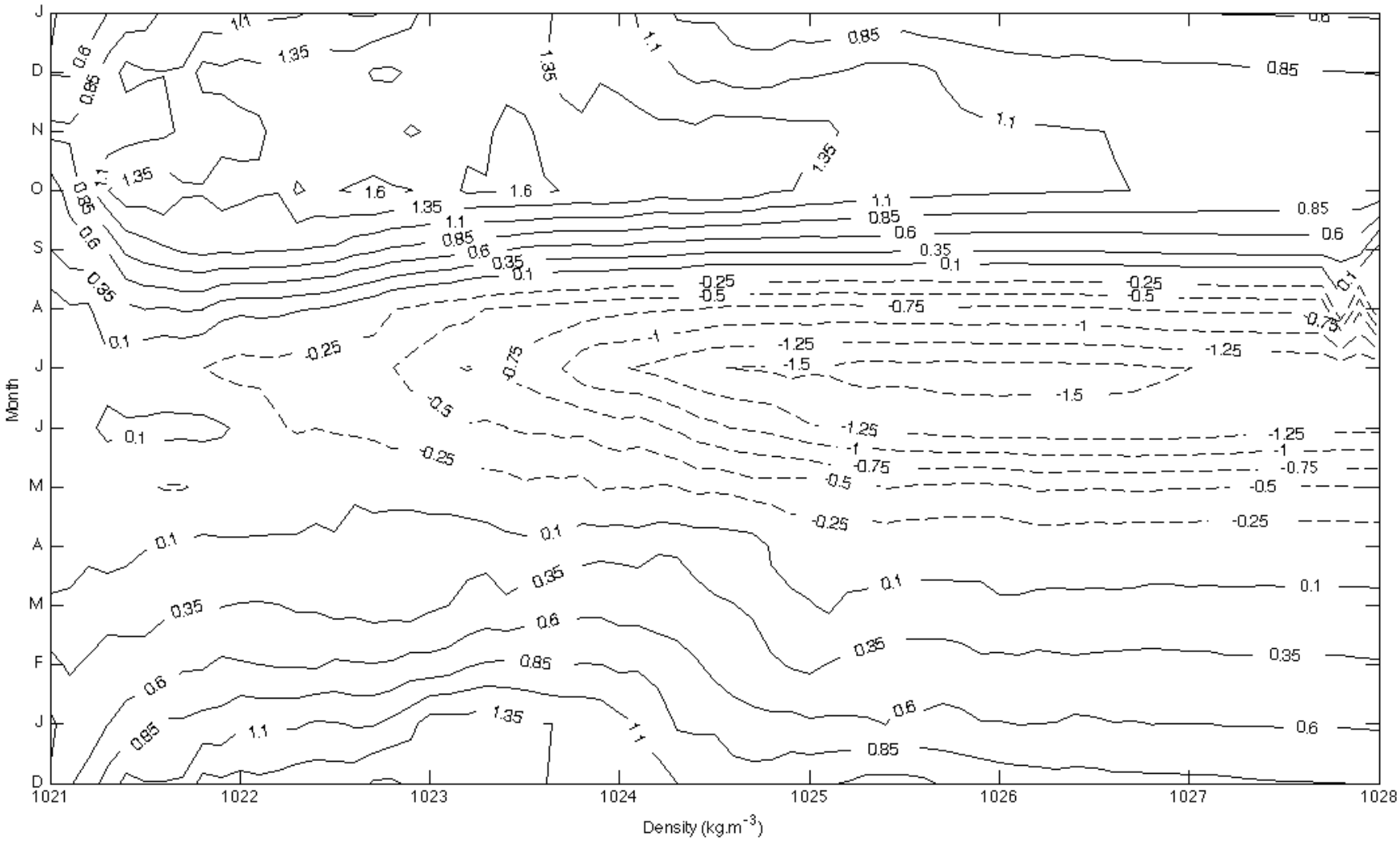

Figure 11: Same as in figure 7, but for the monthly mean J_s^{diab} in the Northern hemisphere. A positive value (solid line) indicates PV destruction and a negative value (dashed line) represents a PV entry.

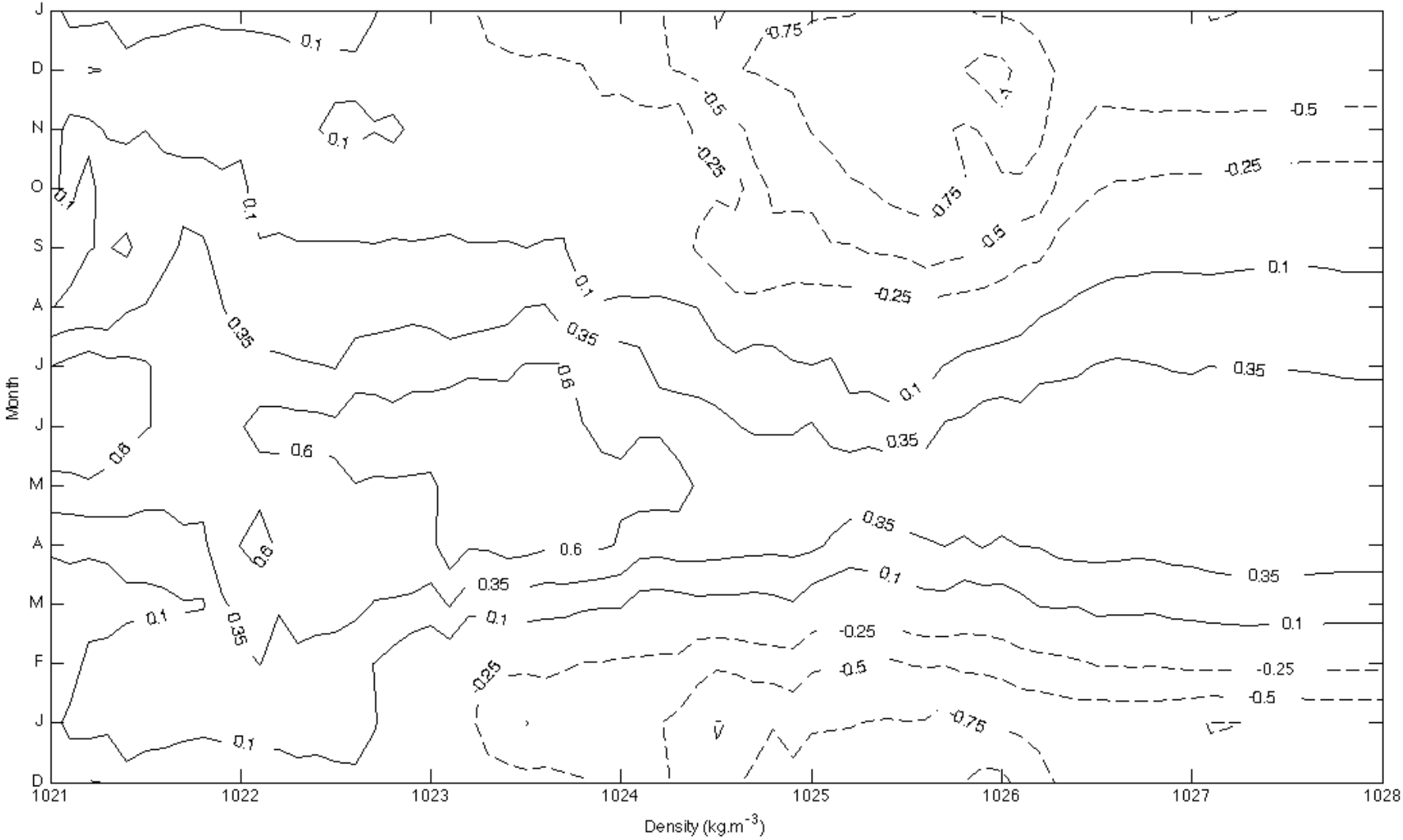

Figure 12: Same as in figure 8, but for the monthly mean J_s^{diab} in the southern hemisphere. A positive value (solid line) indicates PV destruction and a negative value (dashed line) represents a PV entry.

By quickly comparing figure 9 and figure 13, one can notice that the contribution of the diabatic and frictional PV flux are comparable for the Northern Hemisphere for the whole density range. On the other hand, it is very interesting to see that, during local wintertime, the densities for which the J_s^{diab} is minimum, J_s^{frict} is at its maximum.

4. Discussion

Before any interpretation of the results, it is important to point out the weaknesses and limitations of the study that could have an effect on the results of this study. The first point that need to be highlighted is the resolution of the model outputs used for this study. HadGEM model is a low resolution model, which will obviously not be as precise as if the study would have been done with outputs from a high-resolution model such as HiGEM. Using outputs from a high-resolution model would be a good continuity to this project in order to go deeper in our understanding of the role of frictional forces in PV destruction and the formation of mode waters.

The second limitation that must be taken into account when interpreting the results is the large number of fields used to make the calculations: zonal, meridional and vertical velocities, salinity, temperature and surface pressure. Each of these fields have an incertitude associated, which grows when these field are combine together or derivated. The aims of this study is to discuss the respective contribution of J_s^{frict} and J_s^{diab} in the destruction of PV in order to ameliorate our understanding of the formation process of mode waters. It is not the precise quantification of each component in the PV flux equation. This is why this study does not include the calculation of the incertitude attached to the final results.

The last weaknesses of the results mainly affects the isopycnal analysis. Unfortunately, the model outputs used contained cells for closed or semi-closed seas such as the Mediterranean sea or the black sea. As these regions have specific densities, data from these cells can interfere with the data from the open ocean, which is the region the study focuses on. This is why the reader have to keep in mind that any strong features at very high densities cannot be subject to interpretation. Figures from the isopycnal analysis only display the PV flux for densities smaller than 1028 $kg.m^{-3}$ so one cannot be mistaken by features occurring at higher densities. As explained in

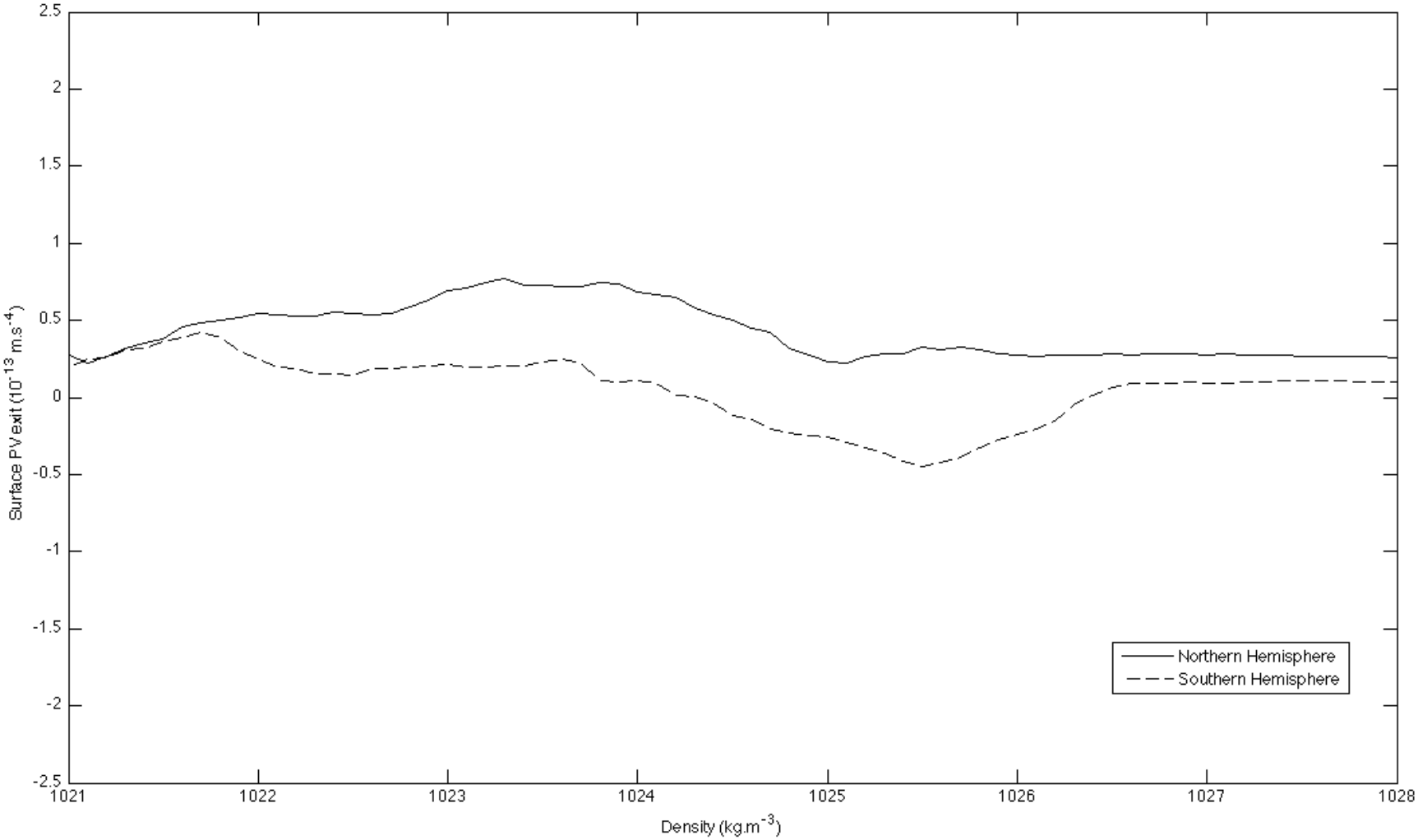

Figure 13: Same as in figure 9 but for the diabatic contribution to the PV flux across the sea surface.

section 1 and can be seen in figure 4, the calculations make a “noise” appear close to the equator. In the vicinity of the equator, the densities are small, this is why the same warning as above can be made for very low densities. Features for densities smaller than 1022 $kg.m^{-3}$ are not necessarily wrong but cannot be trusted enough for a valid interpretation. The different tests detailed in section 2 proved that any results from in-between 1022$kg.m^{-3}$ and 1028 $kg.m^{-3}$ can be trusted in order to make a proper interpretation of the results.

The PV maps (figure 5) show the seasonal variation of the surface PV through a year. The PV is calculated from equation (1). The driving components of this equation are the Coriolis parameter and the vertical gradient of the buoyancy. This is why these maps shows the variation of the Coriolis parameter as a background with features driven by the buoyancy gradient on top. This explains on one hand the fact that the PV decreases equatorward and, on the other hand, the fact that the PV is high during Summer and low during Winter. Indeed, during Wintertime, the PV is at its lowest; no features are visible on top of the background. During Summertime, the surface waters are very stratified which cause the PV to be high.

But during this time of the year, the PV is not high in the whole hemisphere. When it is Summer in the Northern Hemisphere, most of the ocean above 20°N has a very high PV signature, except for specific locations. Indeed, some regions with low-PV signature compared to the rest of the hemisphere can still be identified. These regions, detailed in section 3.2, corresponds to Mode Waters formation locations, identified in Hanawa and Talley (2001). Figure 5.c shows, in the Northern Hemisphere, the low-PV signature of the formation core of the North Atlantic Subpolar Mode Water, the eighteen-degree Mode Water, the Madeira Mode Water and the North Pacific Eastern Sub-Tropical Mode Water. Figure 5.a reveals the low-PV signature of Mode Waters in the Southern Hemisphere; the South Atlantic Sub-Tropical Mode Water off the Brazilian coast, South Pacific Sub-Tropical Mode Water off the Eastern coast of Australia and most of all, the Subantarctic Mode Waters located between 40°S and 60°S.

The latter suggests that the frictional constituent of equation (2) plays a significant role in the destruction of PV. Indeed, during austral summer the diabatic contribution to the PV flux is expected to be negative (PV entry), so the PV at this latitude should increase,

and not stay as low as it is. Figure 10.c confirms that the diabatic component is not responsible for the low-PV signature in this region, as the diabatic PV flux is really small at these latitude in the Southern Hemisphere. Figure 6.c. shows a large upward PV flux due to friction in these latitudes, and thus confirms the fact that, even if the diabatic PV flux seems at first larger than the frictional one, J_s^{frict} can play a crucial role in the destruction of PV.

The comparison of the figures 6 and 10 shows that J_s^{diab} is generally greater than J_s^{frict}, except at low latitudes and around the ACC. This can be explained by the fact that, at low latitudes, the temperature difference between the atmosphere and the ocean is smaller, which results in a weaker diabatic PV flux. But at these same latitudes, westerlies are important and thus lead to an important downward PV flux, as it pushes light water on top of denser water via the Ekman transport. As for the second region, between 40°S and 60°S, it is expected that the frictional PV flux dominates as this region experiences strong winds all year long. The difference between the Southern and the Northern Hemispheres is the presence of land: in the Southern Hemisphere the smaller surface of land allows the winds to be more consistent and stronger, which results in a bigger J_s^{frict}.

The purpose of this study is to investigate how Mode Waters are formed and try to identify the driving mechanism, either diabatic or frictional. Mode Waters being classified by density ranges, an isopycnal analysis reveals to be very informative. Besides, to study the formation of Mode Waters one can focus on the late winter as it is the time when they are thought to be formed, when the seasonal pycnocline suddenly shallows up (Stommel, 1979). This is why figure 9 and figure 13 are the average of J_s^{frict} and J_s^{diab}, respectively, from the month of January to April for the Northern Hemisphere and from July to October for the Southern Hemisphere. This way, it is easier to compare which process is responsible for the formation of Mode Waters.

The first thing to know when analyzing the isopycnal analysis figures is that mode waters have a density contained between 1024 $kg.m^{-3}$ and 1028 $kg.m^{-3}$ (Hanawa and Talley, 2001). So to investigate Mode Waters formation, one must focus on the end of the density range plotted in these figures. The second important point is that, as explained above, Mode Waters are thought to be formed during late winter, so one

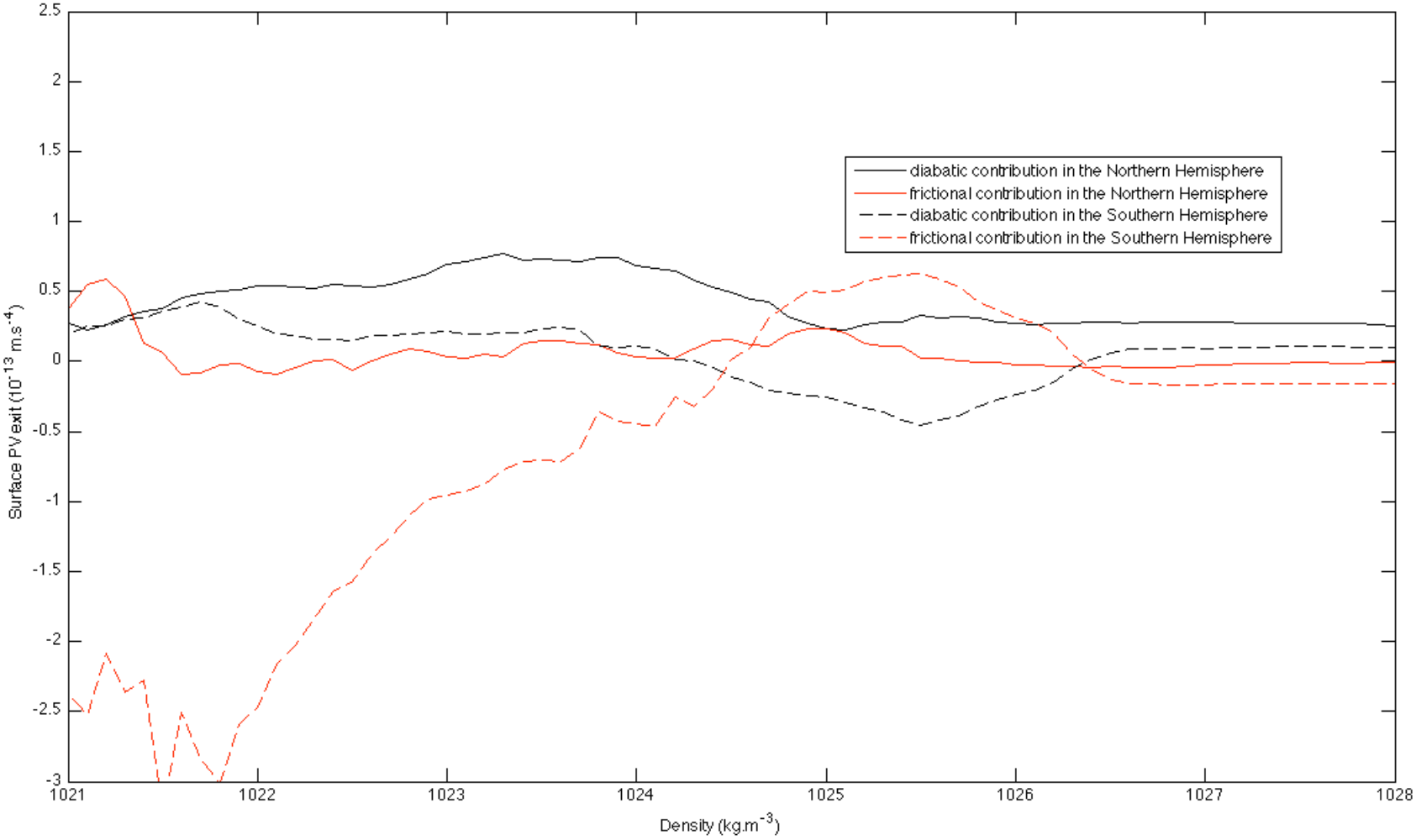

Figure 14: Surface PV exit due to frictional (red line) and diabatic process (black line) in the Northern (solid line) and the Southern (dashed line) Hemisphere average from the month of January to April for the Northern Hemisphere and from July to October for the Southern Hemisphere; in units of 10^{-13} m.s^{-4}.

must also focus on this specific time of the year, which is January through April for the Northern Hemisphere and from July to October for the Southern Hemisphere.

If focusing on the Northern Hemisphere by comparing figures 7 and 11, it appears that the diabatic PV flux dominates for high densities. Figure 7 gives an amplitude in J_s^{frict} mainly around $0.1.10^{-13}$ $m.s^{-4}$, while J_s^{diab} has an amplitude from $0.1.10^{-13}$ $m.s^{-4}$ to $0.6.10^{-13}$ $m.s^{-4}$. It is undeniable that, in this Hemisphere, the diabatic contribution in PV destruction is a lot bigger than the frictional contribution. This could be for two different reasons. First, in the northern Hemisphere the isopycnals migrates a lot through the months, as it can be seen in figure 6 and 10. This means that outcrops can experienced both westerlies and easterlies winds in this season which would weaken the contribution of friction in the destruction of PV for a specific density. And second, winds over the Northern Hemisphere are weaker and less consistent than in the other hemisphere. This results in a smaller frictional PV flux.

But if the same analysis is done for the Southern Hemisphere, by comparing figures 8 and 12, the trend seems to be the opposite. During the austral winter, J_s^{diab} has an amplitude contained between $-0.5.10^{-13}$ $m.s^{-4}$ and $0.1.10^{-13}$ $m.s^{-4}$ for densities higher than 1024 $kg.m^{-3}$. The diabatic component barely destructs PV during the winter. In the meantime, J_s^{frict} has an amplitude from $0.1.10^{-13}$ $m.s^{-4}$ to $0.7.10^{-13}$ $m.s^{-4}$ for the same density range. It is really clear now that in this Hemisphere, the frictional contribution largely dominates on the diabatic contribution to PV destruction. The reasons are the same that the ones cited for the Northern Hemisphere: in the southern hemisphere, outcrops are subject to a smaller spatial migration during wintertime and winds are stronger and more consistent in this part of the globe.

These very interesting observations can be confirmed by figure 14. By looking at this figure, it becomes evident that in the Northern Hemisphere the J_s^{diab} dominates and is mainly responsible for the destruction of PV, thus the formation of Mode waters. In this same figure, it can be seen that for most of the density range, J_s^{frict} largely dominates and is the main mechanism responsible for the destruction of PV. Another interesting feature is the fact that where J_s^{diab} for the Southern Hemisphere reaches its minimum, J_s^{frict} reaches its maximum.

5. Conclusion

As detailed before, the aims of this study was to investigate the role and contribution of each term of the PV flux equation (equation (2)) in the context of formation of Mode Waters, thus destruction of PV. The advective constituent of equation (2) can be ignored as, at the ocean surface, the "impermeability theorem" states that "isopycnal surfaces are impermeable to potential vorticity even in the presence of buoyancy forcing and frictional forces" (Haynes and McIntyre, 1987). Besides, the advective constituent does not play a role in the destruction of PV, it only spreads it horizontally into the upper ocean.

The diabatic component of the PV flux equation has been considered the only responsible for the destruction of PV. The difference in temperature between the atmosphere and the ocean during winter drives diabatic processes at the surface that destruct PV of the upper ocean, thus creates Mode Waters. But lately, the hypothesis that a frictional component could have a significant role in the destruction of PV leaded to new studies trying to prove (Thomas, 2005) and evaluate (Czaja and Hausmann, 2009) this contribution.

This study, based on outputs from the coupled model HadGEM, leads to new conclusions on either J_s^{diab} or J_s^{frict} is the leading constituent of the PV flux equation. There is no simple answer to this problem.

The first conclusion that can be drawn from this study is the fact that in both hemispheres, the contribution of diabatic and frictional processes have the same order of magnitude, contained between $-1.5.10^{-13}$ $m.s^{-4}$ and $1.5.10^{-13}$ $m.s^{-4}$. From this, it can be affirmed that diabatic processes are not the only driving mechanism in the formation of Mode Waters, frictional processes also play a crucial role.

But, in order to know which one dominates, it is very important to separate the two hemispheres. In the Northern Hemisphere, two factors tend to reduce the contribution of J_s^{frict}. The presence of a large landmass limits the winds and the outcrops migration through a year. The frictional PV flux depends a lot on latitudes as winds change direction with latitude. The fact that these outcrops migrates back and forth through a year make them experience both westerlies and easterlies, which decrease and

increase the PV, respectively. These are the main explications why the J_s^{diab} dominates in the Northern Hemisphere, having an amplitude 2 to 5 times bigger than J_s^{frict}.

When Thomas (2001) developed his idea of the under-estimate contribution of frictional processes in the destruction of PV, he stressed the point that this contribution would be even more important in the Southern hemisphere, where the land mass is a lot smaller and outcrops do not migrate as much. This study confirms these hypotheses. It has been found that in the Southern Hemisphere, J_s^{frict} largely dominates the destruction of PV especially along the ACC. In this region during wintertime, the diabatic contribution is barely positive, with a maximum of $0.1.10^{-13}$ $m.s^{-4}$. The frictional contribution can reach seven times that in the same region for the same time of the year, making the destruction of PV via friction processes the main mechanism responsible for the formation of Mode Waters.

We can conclude by saying that both components have their importance, depending on the location. A good sequel of this study would be to do the same calculations for other versions, and resolutions, of the coupled model HadGEM, such as HiGEM. This would provide better results and a way to verify if non-eddy permitting models form Mode Waters in a right way. Indeed, to assess the impact of meso-scale atmospheric features on the diabatic and frictional constituent would help clarify the precise role of each constituent in the formation of Mode Waters.

References:

Brambilla E., and L.D. Talley, 2008: Subpolar Mode Water in the northeastern Atlantic: 1.Averaged properties and mean circulation. *J. Geophys. Res.,* **113**, C04025, doi:10.1029/2006JC004062.

Chelton, D.B., S.K. Esbensen, M.G. Schlax, N. Thum, M.H. Freilich, F.J. Wentz, C.L. Gentemann, M.J. McPhaden, and P.S. Schopf, 2001: Observations of Coupling between Surface Wind Stress and Sea Surface Temperature in the Eastern Tropical Pacific. *J. Climate*, **14**, 1479–1498.

Czaja A. and U. Hausmann, 2009: Observations of Entry and Exit of Potential Vorticity at the Sea Surface. *J. Phys. Oceanogr.*, **39**, 2280-2294.

Hanawa K., and L. D. Talley, 2001: Mode waters. *Ocean Circulation and Climate,* G. Siedler, J. Church, and J. Gould, Eds., International Geophysical Series, Vol. 77, Academic Press, 373–400.

Hanawa K., N. Iwaska, T. Watanabe, T. Suga, and Y. Toba, 1988: The XBT observations. The subtropical mode waters in 1987 winter, *Ocean Research Institute,* University of Tokyo, 46-54.

Haynes P.H., and M.E. McIntyre, 1987: On the evolution of vorticity and potential vorticity in the presence of diabatic heating and frictional or other forces. *J. Atmos. Sci.*, 44, 828-841.

Iselin C.O.D., 1939: The influence of vertical and lateral turbulence on the characteristics of the water at mid-depth. *Trans. Amer. Geophys. Union*, **20**, 414-417.

Marshall, J.C., and A.G. Nurser, 1992: Fluid Dynamics of Oceanic Thermocline Ventilation. *J. Phys. Oceanogr.*, **22**, 583–595.

Qiu, B., and R.X. Huang, 1995: Ventilation of the North Atlantic and North Pacific: Subduction Versus Obduction. *J. Phys. Oceanogr.*, **25**, 2374–2390.

Rhines P.B., 1993: Oceanic general circulation: Wave and advection dynamics. *Modelling Oceanic Climate Interactions,* D. Andersan and J. Willebrandt, Eds., NATO ASI Series, Vol. I, 67-149.

Rhines P.B. and W.R. Young, 1982: A theory of the wind driven circulation. I. Mid-ocean gyres. *J. Mar. Res.*, **40**, 559-596.

Stommel H., 1948: The western intensification of wind driven ocean currents. *Trans. Amer. Geophys. Union*, **29**, 202-206.

Stommel H., 1979: Determination of water mass properties of water pumped down from the Ekman layer to the geostrophic flow below, *Proc. Natl. Acad. Sci. U.S.*, **76**, 3051-3055.

Suga T., Y. Aoki , H. Saito, and K. Hanawa, 2008: Ventilation of the North Pacific subtropical pycnocline and mode water formation. *Progress in Oceanography,* **77**, 285-297.

Talley L.D. and M.S. McCartney, 1982: Distribution and circulation of Labrador Sea Water. *J.Phys. Oceanogr.,* **12**, 1189-1205.

Thomas, L.N., 2005: Destruction of Potential Vorticity by Winds. *J. Phys. Oceanogr.*, **35**, 2457–2466.

Tsubouchi T., T. Suga, and K. Hanawa, 2009: Indian Ocean subtropical mode water: its water characteristics and spatial distribution, *Ocean Sci. Discuss.*, **6**, 723-739.

Wong, A.P.S., and G.C. Johnson, 2003: South Pacific Eastern Subtropical Mode Water. *J. Phys. Oceanogr.*, **33**, 1493–1509.

Worthington L.V., 1959: The 18° Water in the Sargasso Sea. *Deep-Sea Res.*, **5**, 297-305.

Worthington L.V., 1977: Intensification of the Gulf Stream after the winter of 1976-1977. *Nature*, **270**, 415-417.